Optics Letters

Active beam manipulation and convolution operation in VO_2-integrated coding terahertz metasurfaces

ZengLin Li,[1] Wei Wang,[1] Shaoxuan Deng,[1] Jia Qu,[2,4] Yuxiang Li,[1] Bo Lv,[1] Wenjia Li,[1] Xi Gao,[3] Zheng Zhu,[1] Chunying Guan,[1] and Jinhui Shi[1,5]

[1]Key Laboratory of In-Fiber Integrated Optics of Ministry of Education, College of Physics and Optoelectronic Engineering, Harbin Engineering University, Harbin 150001, China
[2]College of Aerospace and Civil Engineering, Harbin Engineering University, Harbin 150001, China
[3]School of Electrical and Information Engineering, Guangxi University of Science and Technology, 545006, Liuzhou, China
[4]e-mail: qujia@hrbeu.edu.cn
[5]e-mail: shijinhui@hrbeu.edu.cn

Received 1 November 2021; revised 24 November 2021; accepted 24 November 2021; posted 1 December 2021; published 14 January 2022

Coding metasurfaces have received tremendous interest due to their unprecedented control of beams through the flexible design of coding sequences. However, realizing tunable coding metasurfaces with scattering-pattern shifts in the terahertz range is still challenging. Here, we propose a VO_2-integrated coding metasurface to realize a thermally controlled scattering-pattern shift by convolution operation. The required phase profiles and high amplitudes of 1-bit and 2-bit coding metasurfaces are easily obtained only by changing the length of the VO_2 cut-wires. The insulator–metal phase transition of the VO_2 cut-wires leads to an ultrafast switching effect between multiple deflected scattering beams and one normally reflected beam. In particular, the VO_2 phase transition contributes to dynamical convolution operations of the 2-bit coding metasurface. The proposed VO_2-integrated coding metasurfaces are important for realizing tunable terahertz beam manipulation as well as arbitrary required scattering beams.

https://doi.org/10.1364/OL.447377

Programmable coding and digital metamaterials offer an unprecedented opportunity to fully control electromagnetic (EM) waves in the temporal, spatial, and frequency domains and have become a powerful platform for realizing various applications [1–3]. In 2014, Cui *et al.* proposed the concept of a coding metasurface with discrete phase elements as metamaterial bits, offering more freedom than material-dependent digital ones [2].

Coding metamaterials provide a flexible platform for manipulating EM waves and realizing many useful phenomena and applications, such as radar cross section (RCS) reduction [2], broadband diffusion [4], the addition theorem and convolution [5,6], the nonlinear Pancharatnam–Berry phase [7], polarization manipulation [8,9], imagers [10], and wireless communications [11]. Remarkably, coding metamaterials readily operate as reprogrammable ones and reconfigurable intelligent surfaces with the introduction of a field-programmable gate array (FPGA) or artificial intelligence algorithms [2,10–12], and are well qualified for switching coding sequences in real time and dynamically manipulating EM waves. In the microwave range, electrically or optically controlled diodes and varactors or graphene can be adopted [2,9–14]. However, diodes and varactors barely work in the terahertz frequency range [4,6,8,15–17]. There are accessible active materials for realizing the dynamic manipulation of terahertz waves, such as Si [18], Ge [8], graphene [19], liquid crystals [20], and vanadium dioxide (VO_2) [21–23]. Several published works reported the dynamic manipulation of terahertz waves [8,15,16], but few attempts have been made to investigate the convolution theorem in active terahertz coding metamaterials for the realization of dynamic scattering-pattern shifts. A bias-encoded VO_2-assisted metasurface for dynamic terahertz wavefront engineering via convolution operation has been proposed [24]; however, biasing three patterned VO_2 layers with different external voltages is difficult. The scattering-pattern shift technique flexibly and continuously manipulates scattering patterns in arbitrarily predesigned directions [6], and even enables scattering patterns of harmonics in any spatial direction at a time-domain digital coding metasurface [25], so it is highly desirable and important to explore tunable and reconfigurable terahertz beam manipulation using the convolution theorem in simplified metamaterials.

In this work, we propose a tunable coding terahertz metasurface to study the switching phenomenon of scattering beams. The coding terahertz metasurface is composed of five single-layer VO_2 cut-wires, a dielectric layer, and a metallic ground layer. By changing the length of the VO_2 cut-wires, both 1-bit coding sequences and 2-bit coding sequences can be designed. The phase transition of the VO_2 cut-wires leads to an ultrafast and dynamical switching effect for scattering beams and dynamical convolution operations of the 2-bit coding metasurface.

VO_2 is one of the most important phase-transition materials that can dynamically modulate EM wave propagation from terahertz to optical frequencies [21,26]. Triggered by external optical, electrical, or thermal stimuli, it undergoes an insulator–metal phase transition on a time scale of several nanoseconds or even picoseconds [21,24]. In order to reduce the bulkiness, tunable mechanism complexity, and fabrication difficulty of the tunable terahertz coding metamaterial, we propose a single-layer microstructured VO_2 coding metamaterial that can be entirely

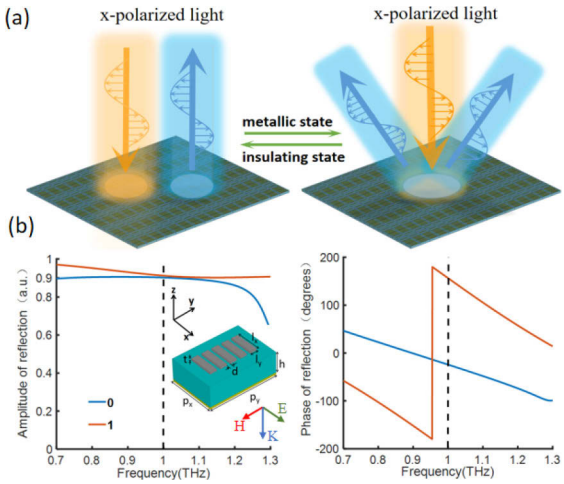

Fig. 1. Schematic of a microstructured VO_2 coding metasurface and phase-transition-assisted beam manipulation. (a) Conceptual illustration of beam switching of normal and anomalous reflection at a VO_2 coding metasurface. (b) Amplitude and phase properties of coding elements "0" (top curve) and "1" (bottom curve) consisting of metallic VO_2 cut-wires. The inset shows the unit cell, which is composed of five identical and parallel cut-wires. The lengths l_x of two coding elements are 22 and 138 μm, respectively.

modulated by external stimuli, as shown in Fig. 1. The metamaterial consists of a microstructured VO_2 layer, an intermediate dielectric spacer, and a metallic ground plane. The intermediate dielectric spacer is polyimide with a height h of 42 μm. The metallic ground plane is a 0.5-μm-thick gold layer that can prevent any transmission of terahertz waves. The microstructured VO_2 layer is composed of an array of five identical and parallel cut-wires, as shown in the inset of Fig. 1. The periodicities of the array are $p_x = 140$ μm and $p_y = 200$ μm, respectively. The thickness of the VO_2 cut-wire is $t = 0.5$ μm. The distance between two adjacent cut-wires is $d = 10$ μm. The width $l_y = 20$ μm of the cut-wire is kept constant, but its length l_x is variable to allow appropriate phase responses to be achieved. The reflection efficiency is always high and a phase range of close to 2π can be achieved for an x-polarized terahertz wave when the length of the cut-wires is varied. The insulator–metal phase transition of the VO_2 is expected to modulate the scattering pattern of the terahertz wave. For simplicity, the required coding sequences may be considered for the metallic state of the VO_2 cut-wire. In this work, digital meta-atoms are designed by varying the length of the VO_2 cut-wire. The commercial software CST Microwave Studio is used to study the reflection phases and amplitudes of the digital coding meta-atoms. When the lengths of the VO_2 cut-wires are 22 and 138 μm, the phase difference between them is about 180°. Hence, these two meta-atoms can be regarded as "0" and "1" elements in a 1-bit digital coding metamaterial.

The terahertz responses of VO_2 can be modeled using the Drude model with frequency-independent conductivity [26]. The insulator-to-metal transition of VO_2 occurs at about 340 K [21]. The conductivity values $\sigma = 1\times10^3$ and 3×10^5 S/m can be adopted to calculate the properties of the complete insulating and metallic VO_2. It is predicted that the desired beam radiation patterns will be achieved in the metallic VO_2 metasurface. The reflection amplitude and phase spectra of the "0" and "1" elements when VO_2 is in a metallic state with conductivity

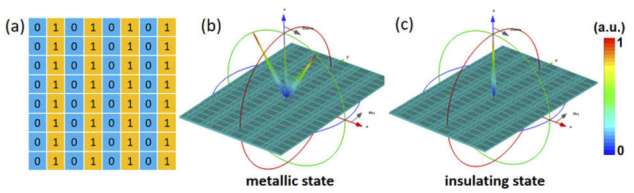

Fig. 2. Schematic of and the switching effect of scattering patterns at a 1-bit coding metasurface with the coding sequence 0101.../0101... at 1 THz. (a) Schematic of the coding sequence. (b) Scattering beam from the 1-bit coding metasurface with metallic VO_2 cut-wires. (c) Scattering beam from the 1-bit coding metasurface with dielectric VO_2 cut-wires.

$\sigma = 3\times10^5$ S/m are shown in Fig. 1(b). As can be seen from Fig. 1(b), the reflection amplitudes of the "0" and "1" elements are 0.902 and 0.912 at 1 THz, respectively. The reflection is very high and the amplitude difference between the two elements is only 0.01, making it suitable for manipulating far-field radiation patterns. The phases of the "0" and "1" elements are −24° and 156.5° at 1 THz, respectively. The phase difference between the two elements is almost 180°. As a result, a 1-bit coding metasurface that can control the radiation patterns according to the coding sequence can be designed. When the temperature is decreased to room temperature, VO_2 enters an insulating state with a conductivity of $\sigma = 1\times10^3$ S/m. The metasurface is equivalent to a metal plate since both the VO_2 pattern and the polyimide layer are transparent to terahertz wave illumination, so the normal reflection effect occurs.

Various coding sequences in coding metasurfaces provide for abundant control of terahertz waves. A 1-bit coding metasurface with the coding sequence 010101.../010101... is first studied, as shown in Fig. 2. The size of the coding metasurface is infinite, with periodic boundary conditions applied in the simulations. The width and length of each lattice are $\Gamma_x = 4\times p_x = 560$ μm and $\Gamma_y = 2\times p_y = 400$ μm, respectively, and each lattice is composed of 2×2 "0" and "1" elements. When all the VO_2 cut-wires are in a metallic state, the normally x-polarized incident beam will mainly be reflected in two symmetrically oriented directions by the metasurface at 1 THz, as shown in Fig. 2(b). The deflection angle θ of the aforementioned coding sequence is determined by $\theta = \arcsin(\lambda/\Gamma_x)$, in which λ is the working wavelength. Γ_x and Γ_y are the lattice periods of the coding sequence. Substituting $\Gamma_x = 560$ μm and $\lambda = 300$ μm into the equation, the resulting reflection angle is 32.4°, and the theoretical value is consistent with that obtained from the simulation. When the VO_2 cut-wires are in an insulating state with a conductivity of 1×10^3 S/m, only the normal reflection beam is generated, as shown in Fig. 2(c). Therefore, the insulator-to-metal phase transition of the VO_2 cut-wire enables the switching effect of scattering patterns.

A 1-bit coding metasurface with the chessboard coding sequence 010101.../101010... will produce four symmetrical scattering beams. The deflection angle θ can be determined via [6]

$$\theta_1 = \arcsin(\lambda/\Gamma_x),\ \theta_2 = \arcsin(\lambda/\Gamma_y),\ \theta = \arcsin\sqrt{\sin^2\theta_1 \pm \sin^2\theta_2}. \quad (1)$$

The chessboard coding sequence is given in Fig. 3(a), and the switching effect (four scattering beams switching to a single scattering beam) is illustrated in Figs. 3(b) and 3(c). Substituting $\Gamma_x = 560$ μm or $\Gamma_y = 800$ μm and $\lambda = 300$ μm into Eq. (1),

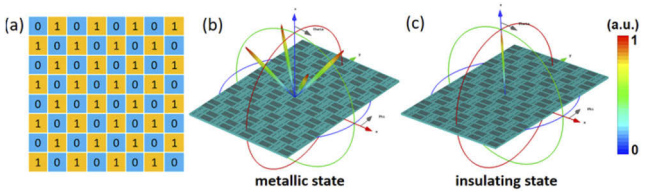

Fig. 3. Schematic of and the switching effect of scattering patterns at a 1-bit coding metasurface with the coding sequence 0101. . . /1010. . . at 1 THz. (a) Schematic of the chessboard coding sequence. (b) Scattering beams from the 1-bit coding metasurface with metallic VO_2. (c) Scattering beam from the 1-bit coding metasurface with dielectric VO_2.

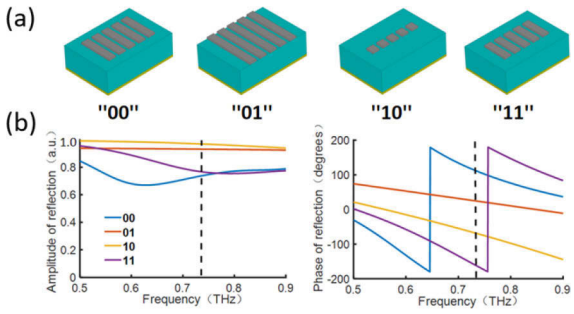

Fig. 4. Amplitude and phase responses of the four coding elements in 2-bit coding metasurfaces with different VO_2 cut-wires. (a) Geometries of the "00," "01," "10," and "11" elements. (b) Amplitude and phase responses of the "00," "01," "10," and "11" elements. From bottom to top, 00, 11, 01, and 10.

the deflected angle θ is calculated as 40.8°, which is consistent with the simulation result. When the VO_2 cut-wires undergo the phase transition from metal to insulator, and a plane terahertz wave illuminates the checkerboard metasurface, a dynamically switching phenomenon can be achieved where four symmetrically scattering beams switch to one normally reflected beam.

The concept of the coding metasurface can easily be extended from 1-bit coding to 2-bit coding, or even higher. Figure 4(a) shows a schematic drawing of the four coding elements in the designed 2-bit coding metasurface. The required amplitude and phase profiles can be realized by changing the length of the VO_2 cut-wires, as shown in Fig. 4(b), where the VO_2 cut-wires are metallic. The VO_2 lengths l_x of the "00," "01," "10," and "11" elements are 91 μm, 140 μm, 22 μm, and 70 μm, respectively. The corresponding phase responses are 114°, 25°, −67°, and −158° at 0.73 THz, respectively. The phase difference between two adjacent coding elements is $\pi/2$, which is well matched with the requirements for the 2-bit coding metasurface. As shown in Fig. 4(b), the amplitudes of the "00," "01," "10," and "11" elements are 0.735, 0.932, 0.97, and 0.77 at 0.73 THz, respectively. This configuration allows the scattering beam to be dynamically adjusted by simply adjusting the temperature of the VO_2 cut-wires.

In order to arbitrarily manipulate the scattering beams of EM waves, Fourier operations are introduced into the 2-bit coding sequence [16]. In this case, for simplicity, the "00," "01," "10," and "11" elements are denoted 0, 1, 2, and 3, respectively, as shown in Fig. 5(a). The gradient coding sequence is 0123. . . /0123. . . . The width and length of each lattice are

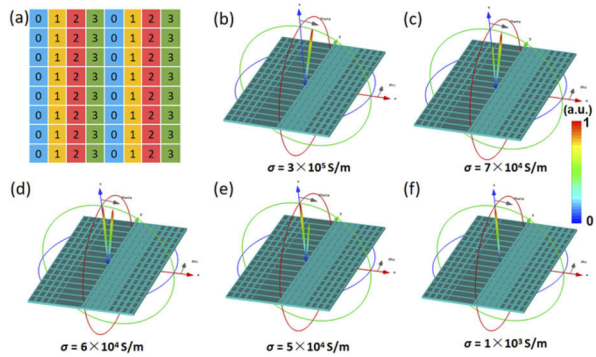

Fig. 5. Schematic of and the switching effect of scattering patterns at a 2-bit coding metasurface with the coding sequence 0123. . . /0123. . . at 0.73 THz. (a) Schematic of the 2-bit coding sequence. (b)–(f) Scattering beam from the 2-bit coding metasurface with $\sigma = 3\times10^5$ S/m, 7×10^4 S/m, 6×10^4 S/m, 5×10^4 S/m, and 1×10^3 S/m.

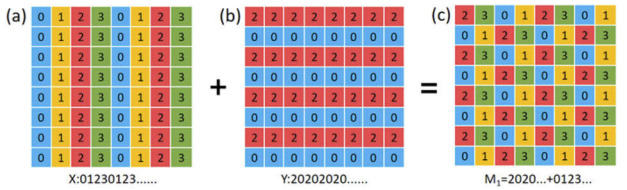

Fig. 6. Convolution operation of the 2-bit coding metasurface.

$\Gamma_x = 16\times p_x = 2240$ μm and $\Gamma_y = 16\times p_y = 3200$ μm, and each lattice is composed of 4×4 "00," "01," "10," and "11" elements. When VO_2 is in a metallic state, for a normally incident terahertz wave, the 2-bit coding metasurface will generate single-beam scattering in a certain direction at 0.73 THz, as shown in Fig. 5(b). The deflection angle θ is 10.5°. When the VO_2 cut-wires are gradually changed to an insulating state, the beam deflected at the 2-bit coding metasurface will switch to a normal reflected beam, as illustrated in Fig. 5.

An example is now presented to show how to achieve a scattering-pattern shift at a tunable coding metasurface using two different coding sequences to produce a scattering beam in a specific direction [7] as seen in Fig. 6. The mixed coding pattern M_1 shown in Fig. 6(c) is obtained by adding the gradient sequence "0123. . . " along the x direction [see Fig. 6(a)] and the periodic sequence "2020. . . " along the y direction [see Fig. 6(b)]. The shifted scattering patterns of M_1 are attributable to both the y-oriented "2020. . . " and the x-oriented "0123. . . " coding sequences. The azimuth angle φ and elevation angle θ of the two scattering beams can be computed by the following equations [6]:

$$\theta = \arcsin\sqrt{\sin^2\theta_1 \pm \sin^2\theta_2},\ \varphi = \arctan(\sin\theta_2/\sin\theta_1), \quad \textbf{(2)}$$

in which θ_1 and θ_2 are the deviation angles corresponding to the two coding sequences along the x and y directions [6], respectively.

When the VO_2 cut-wires are metallic, the four coding elements offer the desired phase profiles with relatively high amplitudes. As we know, the metasurface with the x-oriented "0123. . . " coding sequence produces one deflected scattering beam along the x direction [Fig. 7(a)], while the metasurface with the y-oriented "2020. . . " coding sequence leads to two scattering beams in the

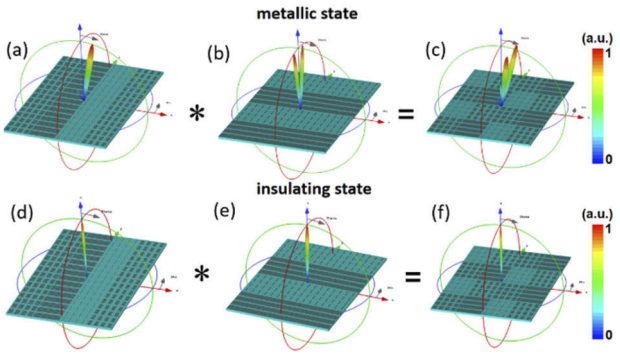

Fig. 7. Schematic of and the switching effect of the scattering-pattern shift at the 2-bit coding metasurface with convolution operations. (a)–(c) Far-field scattering patterns at 2-bit coding metasurfaces with metallic VO_2 cut-wires at 0.73 THz. (d)–(f) Far-field scattering patterns at 2-bit coding metasurfaces with insulating VO_2 cut-wires at 0.73 THz.

yoz plane [Fig. 7(b)]. Furthermore, θ_1 and θ_2 can be calculated as 10.5° and 14.8°, so θ is 18.3°. The azimuth angles φ of the two beams are 54° and 306°, respectively, which are in a good agreement with the numerical simulations. The corresponding scattering patterns in Fig. 7(c) numerically verify that the two scattering beams are deflected from the *yoz* plane without clear distortion, as theoretically expected from the convolution operations. When the VO_2 cut-wires are changed to an insulating state, it is clear from Figs. 7(d)–7(f) that the far-field scattering patterns of the coding metasurface are always a single vertical reflected beam, no matter whether the coding sequence is single or mixed. The above coding methods verify the ability of VO_2 to dynamically control the beam. Based on the above calculations and simulations, dynamical convolution operations on a 2-bit coding metasurface can be realized with the aid of the VO_2 phase transition. This metamaterial design is simple and can be fabricated by film deposition and conventional photolithography [21,23].

In summary, a thermally controlled coding terahertz metasurface has been numerically demonstrated, and the scattering beams can be dynamically switched based on the phase transition of VO_2. The coding metasurface consists of five single-layer parallel VO_2 cut-wires, a dielectric layer, and a metallic ground layer. By adjusting the temperature, the VO_2 cut-wires can be made to undergo an ultrafast phase change from a metallic state to an insulating state, leading to a switching effect where two or four deflected beams switch to a single reflected beam. Remarkably, dynamic convolution operations in the 2-bit coding metasurface can be realized with the aid of the VO_2 phase transition. Flexible and continuous control of terahertz beams at active coding metasurfaces seems to be within reach. In addition, the proposed coding metasurface offers an important scheme with the potential for novel applications in flexible coding devices, terahertz radar antennas, and even orbital angular-momentum-based communications [27].

Funding. National Natural Science Foundation of China (62175049); Natural Science Foundation of Heilongjiang Province (ZD2020F002); 111 project (B13015); Fundamental Research Funds for the Central Universities (3072021CF2508, 3072021CFT2501).

Disclosures. The authors declare no conflicts of interest.

Data availability. Data underlying the results presented in this paper are not publicly available at this time but may be obtained from the authors upon reasonable request.

REFERENCES

1. C. D. Giovampaola and N. Engheta, Nat. Mater. **13**, 1115 (2014).
2. T. J. Cui, M. Q. Qi, X. Wan, J. Zhao, and Q. Cheng, Light: Sci. Appl. **3**, e218 (2014).
3. T. J. Cui, L. L. Li, S. Liu, Q. Ma, L. Zhang, X. Wan, W. X. Jiang, and Q. Cheng, iScience **23**, 101403 (2020).
4. L. H. Gao, Q. Cheng, J. Yang, S. J. Ma, J. Zhao, S. Liu, H. B. Chen, Q. He, W. X. Jiang, H. F. Ma, Q. Y. Wen, L. J. Liang, B. B. Jin, W. W. Liu, L. Zhou, J. Q. Yao, P. H. Wu, and T. J. Cui, Light: Sci. Appl. **4**, e324 (2015).
5. R. Y. Wu, C. B. Shi, S. Liu, W. Wu, and T. J. Cui, Adv. Opt. Mater. **6**, 1701236 (2018).
6. S. Liu, T. J. Cui, L. Zhang, Q. Xu, Q. Wang, X. Wan, J. Q. Gu, W. X. Tang, M. Qi, J. G. Han, W. L. Zhang, X. Y. Zhou, and Q. Cheng, Adv. Sci. **3**, 1600156 (2016).
7. M. L. Ma, Z. Li, W. W. Liu, C. C. Tang, Z. C. Li, H. Cheng, J. J. Li, S. Q. Chen, and J. G. Tian, Laser Photonics Rev. **13**, 1900045 (2019).
8. J. Li, Y. T. Zhang, J. N. Li, X. Yan, L. Liang, Z. Zhang, J. Huang, J. H. Li, Y. Yang, and J. Q. Yao, Nanoscale **11**, 5746 (2019).
9. C. Huang, B. Sun, W. Pan, J. Cui, X. Wu, and X. Luo, Sci. Rep. **7**, 42302 (2017).
10. L. L. Li, H. X. Ruan, C. Liu, Y. Shuang, A. Alu, C. W. Qiu, and T. J. Cui, Nat. Commun. **10**, 1082 (2019).
11. L. Zhang, M. Chen, W. Tang, J. Y. Dai, L. Miao, X. Y. Zhou, S. Jin, Q. Cheng, and T. J. Cui, Nat. Electron. **4**, 218 (2021).
12. L. Zhang, X. Q. Chen, S. Liu, Q. Zhang, J. Zhao, J. Y. Dai, G. D. Bai, X. Wan, Q. Cheng, G. Castaldi, V. Galdi, and T. J. Cui, Nat. Commun. **9**, 4334 (2018).
13. J. Zhang, H. Zhang, W. Yang, K. Chen, X. Wei, Y. Feng, R. Jin, and W. Zhu, Adv. Opt. Mater. **8**, 2000683 (2020).
14. X. G. Zhang, W. X. Jiang, H. L. Jiang, Q. Wang, H. W. Tian, L. Bai, Z. J. Luo, S. Sun, Y. Luo, C. W. Qiu, and T. J. Cui, Nat. Electron. **3**, 165 (2020).
15. J. H. Li, Y. T. Zhang, N. Ji, J. Li, Y. Yang, J. Huang, C. Q. Ma, Z. Z. Ma, Z. Zhang, L. J. Liang, and J. Q. Yao, Opt. Commun. **458**, 124744 (2020).
16. L. Y. Wang, F. Lan, Y. X. Zhang, S. X. Liang, W. X. Liu, Z. Q. Yang, L. Meng, Z. J. Shi, J. Yin, T. T. Song, H. X. Zeng, and P. Mazumder, Opt. Express **28**, 6395 (2020).
17. X. Fu, F. Yang, C. Liu, X. Wu, and T. J. Cui, Adv. Opt. Mater. **8**, 1900628 (2020).
18. H.-T. Chen, J. F. O'Hara, A. K. Azad, A. J. Taylor, R. D. Averitt, D. B. Shrekenhamer, and W. J. Padilla, Nat. Photonics **2**, 295 (2008).
19. S. H. Lee, M. Choi, T. T. Kim, S. Lee, M. Liu, X. B. Yin, H. K. Choi, S. S. Lee, C. G. Choi, S. Y. Choi, X. Zhang, and B. Min, Nat. Mater. **11**, 936 (2012).
20. D. Shrekenhamer, W. C. Chen, and W. J. Padilla, Phys. Rev. Lett. **110**, 177403 (2013).
21. M. K. Liu, H. Y. Hwang, H. Tao, A. C. Strikwerda, K. Fan, G. R. Keiser, A. J. Sternbach, K. G. West, S. Kittiwatanakul, J. Lu, S. A. Wolf, F. G. Omenetto, X. Zhang, K. A. Nelson, and R. D. Averitt, Nature **487**, 345 (2012).
22. T. T. Lv, G. H. Dong, C. H. Qin, J. Qu, B. Lv, W. J. Li, Z. Zhu, Y. X. Li, C. Y. Guan, and J. H. Shi, Opt. Express **29**, 5437 (2021).
23. M. Liu, Q. Xu, X. Y. Chen, E. Plum, H. Li, X. Q. Zhang, C. H. Zhang, C. W. Zou, J. G. Han, and W. L. Zhang, Sci. Rep. **9**, 4097 (2019).
24. J. Shabanpour, S. Beyraghi, and A. Cheldavi, Sci. Rep. **10**, 14920 (2020).
25. C. Zhang, J. Yang, L. X. Yang, J. C. Ke, M. Z. Chen, W. K. Cao, M. Chen, Z. H. Wu, J. F. Chen, Q. Cheng, and T. J. Cui, Nanophotonics **9**, 2771 (2020).
26. F. Ding, S. Zhong, and S. I. Bozhevolnyi, Adv. Opt. Mater. **6**, 1701204 (2018).
27. K. Zhang, Y. Yuan, X. Ding, H. Li, B. Ratni, Q. Wu, J. Liu, S. N. Burokur, and J. Tan, Laser Photonics Rev. **15**, 2000351 (2021).